Ionic Binding of Na^+ versus K^+ to the Carboxylic Acid Headgroup of Palmitic Acid Monolayers Studied by Vibrational Sum Frequency Generation Spectroscopy†

Cheng Y. Tang and Heather C. Allen*

The Ohio State University, Department of Chemistry, 100 West 18th Avenue, Columbus, Ohio 43210

Received: January 3, 2009; Revised Manuscript Received: April 24, 2009

Ionic binding of alkali ions Na^+ and K^+ to the carboxylic acid headgroups of fatty acid monolayers is studied as a proxy toward understanding the fundamental chemistry in cell biology. In this study, we used broad-bandwidth sum frequency generation (BBSFG) vibrational spectroscopy to investigate the ionic binding event that leads to deprotonation and complex formation of fatty acid headgroups. Palmitic acid ($C_{15}H_{31}COOH$) exists as a monolayer on aqueous surfaces. Surface vibrational stretch modes of palmitic acid from 1400 cm^{-1} to 3700 cm^{-1} were observed (ν_s-COO^-, ν-C═O, ν-C—H, ν-O—H of —COOH, free OH). Palmitic acid is mostly protonated at the aqueous surface at neutral pH (~6). However, various degrees of deprotonation are initiated by the introduction of Na^+ and K^+ that results in the complexation of K^+:COO^- and solvent separated Na^+:COO^-. Evidence in several spectral regions indicates that K^+ exhibits stronger ionic binding affinity to the carboxylate anion relative to Na^+.

1. Introduction

Alkali cation binding events in aqueous solution are of great interest in biology and, more specifically, in neuroscience. Sodium and potassium are the major ionic components of intra- and extracellular fluids, and their function is critical in electrical communication across cell membranes.[1] However, even though they possess similar chemical properties by belonging to the same chemical group, pronounced selectivity differences are observed in cross-membrane transport and remain to be addressed.[1,2] To this end, Langmuir monolayers at the air—aqueous interface have long been a popular model system for biological membranes.[3] For instance, studies that encompass molecular structures,[4–6] film morphologies,[7–9] and molecular interactions[4,10] have been attempted. Additionally, long-chain fatty acids are most frequently used as standard materials in applied surfactant monolayer studies.

On the basis of informative techniques that are used in Langmuir monolayer studies at the air—aqueous interface, different aspects of monolayer properties can be obtained. For example, surface compression isotherms provide macroscopic phase information about monolayers under constant compression;[11] Brewster angle microscopy (BAM) and fluorescence microscopy provide visual images of film morphologies in different phases;[7–9] grazing incidence X-ray diffraction (GIXD) directly probes molecular structures in crystalline phases in terms of different forms of aliphatic chain packing;[5] and infrared reflection absorption spectroscopy (IRRAS) not only helps in determining surface molecular species but also provides molecular structural information such as the molecular conformation and chain orientation via spectral analysis.[10,12] Among all of these, the first two techniques probe macroscopic information, whereas the last two probe microscopic information at the molecular level, however, with limited sensitivities. GIXD has a low scattering response from monolayers, while IRRAS is intrinsically a linear technique; that is, the intensity response is linearly dependent on the molecular density within the monolayer.

Thus far, in the surface science community, IRRAS has been the predominant technique employed as a direct probe in studies of ionic binding of aqueous phase cations to fatty acid headgroups. After pioneering structural investigations of monolayers at the air—water interface using IRRAS introduced by Dluhy and Cornell,[13] Gericke et al. later used the same technique to study the ionic binding of stearic acid ($C_{17}H_{35}COOH$) with aqueous divalent cations (Ba^{2+}, Cu^{2+}, Ni^{2+}, and Zn^{2+}).[10] With the addition of polarization modulation to IRRAS, Le Calvez et al. studied both divalent and monovalent cations (Cd^{2+}, Ca^{2+}, Mg^{2+}, and Na^+) with respect to a deuterated arachidic acid ($C_{19}D_{39}COOH$) monolayer at the air—aqueous interface under different pH conditions.[14] Even though ionic binding of cations in the aqueous phase to fatty acid monolayers has been studied extensively by using IRRAS, it is evident that both molecular sensitivity and spectral signal-to-noise continue to be limiting factors. By using vibrational sum frequency generation (VSFG) spectroscopy, Miranda et al. were the first to study the deprotonation effect of an arachidic acid monolayer under basic conditions, which emphasized water structure under the influence of the monolayer.[15] Miranda et al. did not address ionic binding to the monolayer. Cremer et al. also studied water structure in different phases of surfactant monolayer coverage on subphases that contain Hofmeister anions.[16,17] The main objective was to interrogate the behavioral trend of these anions affecting the adjacent water structure because of direct ionic interactions. Recent SFG studies have covered areas such as ionic adsorption of surfactant salts at the liquid—solid interface by Richmond and co-workers[18] and ionic binding of Na^+ and Ca^{2+} to monolayers of phospholipids by Bonn and co-workers.[19] Very recently, cation-specific (Na^+ and K^+) effects on the hydrogen bonding of the interfacial water structure was investigated by Wang and his co-workers.[20,21] Aside from SFG, second harmonic work by Geiger and co-workers directly probed surface acidity, potential, and charge densities of a —COOH functionalized surface under the influence of aqueous divalent cations.[22] In addition, experimental work with support of

† Part of the "Robert Benny Gerber Festschrift".

* To whom correspondence should be addressed. E-mail: allen@chemistry.ohio-state.edu.

10.1021/jp9000434 CCC: $40.75
Published on Web 05/19/2009

molecular dynamic simulations and quantum chemistry calculations by Jungwirth and co-workers discussed interactions between macromolecules and ions, specifically, the Hofmeister series ions with an emphasis on the postulate of the "law of matching water affinities" by Collins.[23,24]

In this study, we have applied the VSFG technique to systematically investigate the ionic binding events of biologically relevant cations Na^+ and K^+ to palmitic acid ($C_{15}H_{31}COOH$, PA) monolayers at air−aqueous interfaces. VSFG provides nonlinear vibrational resonant enhancement and surface specificity.[25] Vibrational modes investigated in this study consist of the symmetric stretch of the carboxylate anions, the carbonyl stretch, the C−H stretch, and the O−H stretch of water (dangling OH) and of PA headgroups. Of primary importance is the finding of the distinct K^+ binding characteristics to the PA monolayer as opposed to Na^+. To complement the existing knowledge on ionic binding at air−aqueous interfaces, the findings obtained in this study may provide new insight on the ionic binding of simple alkali ions during transport across biological membranes. The results presented here are in opposition to two recent X-ray absorption spectroscopic (XAS) findings reported separately by Saykally and co-workers[26] and Winter and co-workers.[27] We find that K^+ is much more effective at binding to the carboxylic acid relative to Na^+. A 1:1 ionic complex of K^+ with deprotonated $-COO^-$ is directly observed from VSFG spectra.

2. Vibrational Sum Frequency Spectroscopy

VSFG spectroscopy is a second-order optical technique that demonstrates surface specificity and molecular-level sensitivity.[25,28] As a surface probe, an SFG response is generated by coupling two intense laser pulses overlapped at an interface both temporally and spatially. Under the electric-dipole approximation, the SFG response must vanish in centrosymmetric media.[25] This naturally makes SFG a surface specific technique since centrosymmetry breaks down at the surface; therefore, a lack of centrosymmetry in molecules also becomes a part of the SFG selection rules. In theory, the SFG field originates from the second-order polarization, which makes the SFG intensity proportional to the square of the polarization, as shown in eq 1.

$$I_{\mathrm{SFG}} \propto |P^{(2)}|^2 \propto |\chi_{\mathrm{NR}}^{(2)} e^{i\phi_{\mathrm{NR}}} + \sum_v \chi_v^{(2)}|^2 I_{\mathrm{vis}} I_{\mathrm{IR}} \qquad (1)$$

$P^{(2)}$ is the second-order polarization of the medium; $\chi_{\mathrm{NR}}^{(2)}$ and $\chi_v^{(2)}$ are the nonresonant and the resonant second-order nonlinear susceptibilities, respectively; ϕ_{NR} is the nonresonant phase term; and I_{vis} and I_{IR} are the intensities of the incident visible and infrared pulsed lasers. The resonant enhancement occurs when the frequency of the incident infrared laser beam is resonant with a vibrational mode of a molecule, which is directly shown in eq 2.

$$\chi_v^{(2)} \propto \frac{A_v}{\omega_{\mathrm{IR}} - \omega_v + i\Gamma_v} \qquad (2)$$

A_v is the transition moment strength, ω_{IR} is the incident infrared frequency, ω_v is the frequency of the vibrational transition, and Γ_v is the line width of the vibrational transition, also known as the half-width at half-maximum (hwhm). Because the underlying process involved in SFG is coherent anti-Stokes Raman scattering from a vibrationally excited state, A_v has a combined contribution from the transition moment strength of the infrared transition and the Raman transition, in which case this becomes an SFG spectroscopic selection rule. That is to say, the resonant-enhanced vibrational mode has to be both infrared and Raman active. Since $\chi_v^{(2)}$ represents a macroscopic optical property of the medium, it naturally has its molecular origins in the molecular hyperpolarizability, β_v. Via an ensemble average of the Euler angle transformation between the molecular coordinate and the laboratory coordinate, $\chi_v^{(2)}$ is directly related to β_v by the number density of the molecular groups, as shown in eq 3.

$$\chi_v^{(2)} = N \sum_{lmn} \langle \mu_{IJK:lmn} \rangle \beta_v \qquad (3)$$

N is the number density, and $\langle \mu_{IJK:lmn} \rangle$ is the Euler angle transformation between the molecular coordinate, *lmn*, and the laboratory coordinate, *IJK*.

SFG is also a versatile polarization probe that can demonstrate quantitative structural information related to conformational order, molecular orientation, and anisotropy. Under the assumption of $C_{\infty v}$ symmetry of a given isotropic interface, seven tensorial elements of $\chi_v^{(2)}$ are nonvanishing, out of 27 potential tensorial elements. If the plane of incidence is chosen to be the $x-z$ plane and the $x-y$ plane is chosen to be the interface, only three unique values of $\chi_v^{(2)}$ are possible among those seven nonvanishing tensorial elements under the condition of off-resonance from the visible beam. These three unique values are demonstrated by the following relations: $\chi_{xxz}^{(2)} = \chi_{yyz}^{(2)}$, $\chi_{xzx}^{(2)} = \chi_{yzy}^{(2)} = \chi_{zxx}^{(2)} = \chi_{zyy}^{(2)}$, $\chi_{zzz}^{(2)}$. To probe these three values, it is necessary to use the polarization combinations of ssp, sps, and ppp; individually, these are represented by the three available photons in the order of increasing wavelength, that is, SFG, visible, and infrared.

3. Experimental Section

3.1. Materials. PA (>99% purity) and acyl chain deuterated PA (>98% purity) were purchased from Sigma-Aldrich and Cambridge Isotope, respectively. Both corresponding solutions were prepared in the 1.5 mM concentration range by dissolving in spectroscopic-grade chloroform that was purchased from Sigma-Aldrich. Sodium chloride (certified ACS, 99% purity) and potassium chloride (EP/BP/USP/FCC, 99% purity) were purchased from Fisher Scientific to prepare stock solutions by dissolving in deionized water (18.2 MΩ·cm resistivity) from a Barnstead Nanopure system at pH of 6.0.

Stock solutions of sodium chloride and potassium chloride were filtered using a Whatman Carbon-Cap activated carbon filter to eliminate potential organic contaminants. The concentrations of the filtered stock solutions were standardized on the basis of the Mohr titration technique,[29] in which silver nitrate (reagent grade) and potassium chromate (99.5% purity) were applied as a titrate and an indicator, respectively; their respective suppliers were Fisher Scientific and E.M. Science. To replicate standard saline concentrations in seawater and biological systems, 0.6 and 0.2 M salt solutions were chosen respectively in this study and then prepared by dilutions of desired amounts of stock solutions. In the pH studies, manipulation of pH values in the water subphase was controlled by mixing an appropriate amount of concentrated HCl or NaOH solution (reagent grade, Fisher Scientific) by direct pH meter readings (Accumet Basic AB15, Fisher Scientific). In addition, all solutions were conditioned at room temperature (23 ± 1 °C) over 24 h.

3.2. Methods. ***3.2.1. Langmuir Film Balance.*** The surface compression isotherm ($\pi-A$) was acquired by a KSV minitrough (KSV, Finland) with dimensions of 176.5 mm × 85 mm. The trough and the two barriers are made of Teflon and Delrin, respectively. During compression, the $\pi-A$ isotherms were recorded in real time by the Wilhelmy plate method. After 24 h equilibration at room temperature, the monolayer−subphase systems were maintained at 23 °C. The surface was compressed quickly and examined for any sign of surface pressure increase to ensure negligible organic contamination prior to spreading the PA monolayer. After confirming the surface purity, tens of microliters of PA−chloroform solution were spread in a dropwise fashion by a microsyringe (Hamilton) for homogeneous spreading. Ten minutes was allowed for complete solvent evaporation. During compression, a constant rate of 5 mm/min of both barriers was employed.

3.2.2. Monolayer at Equilibrium Spreading Pressure. Monolayers at equilibrium spreading pressure (ESP) were spread over the various solutions in Petri-dishes, which underwent a stringent cleaning procedure: first, soaking in concentrated sulfuric acid with an addition of strong oxidizer, ammonium peroxidisbisulfate, for 2−3 h and then rinsing thoroughly with a copious amount of nanopure water before drying in an oven at 125 °C. The monolayers of PA at ESP on neat water and the salt solutions were able to attain a mean molecular area (MMA) coverage of ∼21 $Å^2$/molecule, which are generally assumed to be in a highly ordered 2D phase. After spreading, 10 min was also allowed for solvent evaporation and monolayer stabilization. Then, VSFG spectra were acquired in the spectral region of interest for both structural and chemical information.

3.2.3. VSFG Spectrometer (Broad Bandwidth Technique). The broad bandwidth VSFG spectrometer setup has been thoroughly described elsewhere.[30] Here, only a concise introduction is given. A titanium:sapphire oscillator (Spectra-Physics, Tsunami) with an optimal center wavelength at 792 nm and a sub-50 fs pulse width seeds two 1 kHz regenerative amplifiers (Spectra-Physics, Spitfire, femtosecond and picosecond versions) that are pumped by a solid state Nd:YLF laser (Spectra-Physics, Evolution 30) at 527 nm. The resulting laser beams from the two respective regenerative amplifiers are 85 fs pulses at 792 nm (22 nm bandwidth) and 2 ps pulses at 792 nm (17 cm^{-1} bandwidth). For the tunable broadband infrared laser generation in an optical parametric amplifier (Light Conversion, TOPAS), the broadband femtosecond laser pulses are used to generate amplified parametric waves (signal and idler) via a BBO (beta barium borate) crystal using three general steps: superfluorescence generation, preamplification, and power amplification of the signal beam. The amplified signal and idler beams are then used to create an infrared beam via a $AgGaS_2$ crystal in the nonlinear difference−frequency generation system (Light Conversion, NDFG connected to the TOPAS). On average, the spectral bandwidth (fwhm) of the resultant broadband infrared beam is 200 cm^{-1} in the spectral regions under investigation, and because it is a broadband infrared pulse, good signal-to-noise ratio VSFG spectra are acquired for durations ranging from 30 to 300 s depending on the cross sections of the vibrational modes of interest. The output of the infrared beam can easily cover from 1000 to 4000 cm^{-1} with sufficient energy outputs as predicted by tuning curves for BBO (type II phase matching) and $AgGaS_2$ (type I phase matching) crystals and the crystal nonlinear efficiencies. For instance, the average infrared energies at the sample stage in this study were measured to be 5, 6, 10, and 8 μJ in the spectral regions of ν_s-COO^- (1350−1550 cm^{-1}), ν-CO (1600−1800 cm^{-1}), ν-CH (2800−3000 cm^{-1}), and ν-OH (3500−3800 cm^{-1}), respectively. Furthermore, to minimize an energy loss of the infrared beam and an overwhelming spectral interference from water vapor absorption, 95% of the infrared beam path was purged with dry nitrogen gas (in-house). Additionally, 300 and 350 μJ visible energies and variations of infrared energies were utilized for VSFG energy tests to ensure the SFG response that correctly corresponds with eq 1.

As mentioned in the previous section, the probe beams consisting of the 792 nm visible beam and the broadband infrared beam need to overlap at the sample surface spatially and temporally for the SFG process. The generated VSFG signal from the sample surface is detected in reflection via a combination of two optical components: first, a monochromator (Acton Research, SpectraPro SP-500 monochromator with a 1200 g/mm grating blazed at 750 nm) for the spectral dispersion and then a liquid-nitrogen cooled charge-coupled device (CCD) camera (Roper Scientific, 1340 × 400 pixel array, LN400EB back illuminated CCD) for signal collection. During this study, polarization investigation was also implemented. Polarization combinations of ssp (s-SFG; s-visible; p-infrared), sps, and ppp were used. To arrive at the final VSFG spectra presentation, background-subtracted VSFG spectra were normalized against the broadband infrared beam energy profile using a nonresonant VSFG spectrum from a GaAs crystal (Lambda Precision Optics, Inc.). The purpose of doing the normalization is to eliminate the spectral distortion caused by the infrared beam energy distribution associated with each frequency in the spectral region of interest. Spectral calibration of VSFG peak positions was completed by comparing the polystyrene absorption bands obtained from a nonresonant GaAs spectrum to reference Fourier transform infrared spectra. By doing this, the VSFG peak positions reported here are accurate to 1 cm^{-1}.

4. Results and Discussion

4.1. PA Compression Isotherms. Phase information of Langmuir monolayers is revealed in their corresponding compression isotherms. In this study, the compression isotherms of the PA monolayers spread on aqueous subphase surfaces were investigated. The subphases include pure (neat) water, Na^+(aq) solutions (0.2 and 0.6 M), and K^+(aq) solutions (0.2 and 0.6 M). Figure 1A,B shows the respective compression isotherms of PA on the Na^+(aq) and K^+(aq) solutions. For comparison, the PA isotherm on neat water is given as a reference. In looking at the isotherms, similarities exist. For instance, the observed trend of the PA monolayer phase transitions under compression (right to left in the isotherm) follows this order: the gas (G)/tilted condensed (TC) coexisting phase → the TC phase → the untilted condensed (UC) phase → the collapsed (C) phase. A second order phase transition appears as a kink on the isotherms when the PA monolayers transition from the TC to the UC phase.[31] During the compression, the initial surface pressure rise occurs at 21 $Å^2$/molecule on the neat water and Na^+(aq) solutions; however, a slight deviation is shown for the 0.2 and 0.6 M K^+(aq) solutions in which a slightly larger MMA is observed at 22 and 23 $Å^2$/molecule, respectively. In addition, the surface pressure at collapse increases when the subphase is varied from the neat water to the Na^+(aq) and K^+(aq) solutions. The surface pressure at the collapse also increases when the concentration of the Na^+(aq) and K^+(aq) solutions is increased. Upon taking a closer look, the reverse trend is found for the surface pressure where the TC to UC phase transition occurs. At this point, the surface pressure slightly decreases for the Na^+(aq) solutions and decreases more for the K^+(aq) solutions

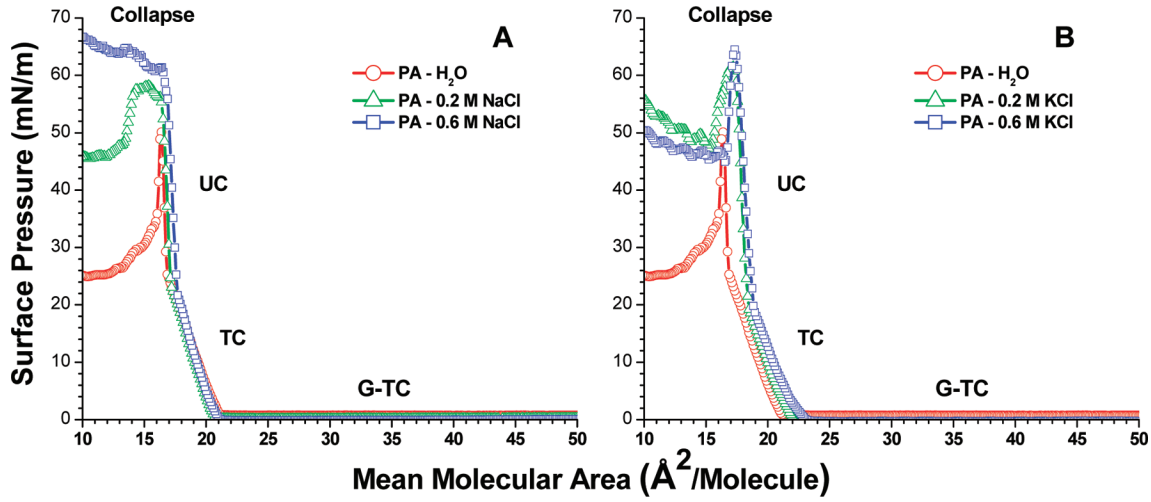

Figure 1. Surface compression isotherms ($\pi-A$) of the PA monolayer at 23 °C on aqueous surfaces: (A) neat water and NaCl (0.2 and 0.6 M) and (B) neat water and KCl (0.2 and 0.6 M).

with respect to the neat water subphase. The same trend, decreasing surface pressure at the collapse, also correlates with the decreasing concentration of same salt solutions.

Because of having only a single saturated hydrocarbon chain, PA can exhibit relatively high compressibility characteristics. In addition, PA forms a highly ordered and compact molecular monolayer in the TC and UC phases as reported in the literature.[32] An MMA of 21 Å^2/molecule is typical for saturated long-chain fatty acids,[33] which indirectly reflects the close-packed nature of the chain when it is subjected to compression. PA is assumed to orient perpendicular to the water surface in the UC phase.[5] In evaluating the slight difference in MMA values of the PA monolayers on the K^+(aq) solutions with respect to water and the Na^+(aq) solutions, it is likely that K^+ and Na^+ interact differently with the headgroup of PA, which constitutes the essence of this study. Furthermore, the different interaction behaviors between the two cations with regard to the headgroup could account for the observed trend of decreasing surface pressure at the TC to UC phase transition as shown in the isotherms.

It is important to note the distinct behavioral contrast of these two cations in cross-membrane transport. It has been postulated that the ionic size and the corresponding binding sites provided by chelating ligands work synergistically in governing the observed selectivity and kinetics differences as reported in the literature.[1] Both cations are conventionally thought to be buried deeply into the bulk and surrounded by hydration shells, but clearly the isotherms are suggestive of differing interfacial activity in the presence of a monolayer.

4.2. VSFG Spectroscopic Data of the PA Monolayers. To decipher the underlying governing factors that have resulted in the small discrepancies revealed in the compression isotherms of the PA monolayers on both neat water and salt solutions, VSFG was employed for its surface specificity and molecular-level sensitivity. In the following studies, spectral regions of interest in relation to the dominant normal modes of vibration of PA are systematically probed. An in-depth understanding is then gained on the basis of spectral differences. The investigated vibrational modes consist of the C—H stretch, the carboxylate ($-COO^-$) symmetric stretch, the carbonyl (C=O) stretch, and the O—H stretch.

4.2.1. C—H Stretching Region (2800−3000 cm^{-1}). As a first step, the VSFG spectra of the PA monolayers in the C—H stretching region were acquired on neat water, Na^+(aq), and K^+(aq) solutions, respectively. All three polarization combinations (ssp, sps, and ppp) were implemented. As shown in Figure 2, at ESP the PA monolayers reveal many dominant spectral peaks on both the water and the salt solutions. The observed peaks, in the order of increasing vibrational frequency, are described in Table 1. Using the ssp polarization combination, three peaks with varying intensities are revealed in each spectrum. These peaks correspond to the methylene symmetric stretch (ν_s-CH_2), the methyl symmetric stretch (ν_s-CH_3), and the methyl Fermi resonance (ν_{FR}-CH_3) at frequencies of 2842, 2872, and 2940 cm^{-1}, respectively. The shoulder at 2960 cm^{-1} in column A is attributed to the methyl asymmetric stretch (ν_a-CH_3). In the sps polarization spectra, only one dominant peak occurs at 2960 cm^{-1}, which corresponds to the ν_a-CH_3. Upon taking a closer look, a small peak is barely resolvable at 2910 cm^{-1} where the methylene asymmetric stretch (ν_a-CH_2) is considered to be the main contributor. In the ppp polarization spectra, the ν_a-CH_3 peak is most intense while the peak intensities from the ν_s-CH_3 and ν_a-CH_2 vibrational modes are fairly weak. Overall, the absolute peak intensities of the aforementioned vibrational modes are similar even though different subphases are used, namely, the neat water, Na^+(aq), and K^+(aq) solutions. This observation is consistent with the mostly similar results obtained from the compression isotherms, in which an overall resemblance exists between Na^+ and K^+, yet small discrepancies are also noticeable. Given the small variations on peak intensities, it is difficult to infer any firm conclusion regarding a behavior difference on the interactions between Na^+ and K^+ with the headgroup of PA based solely on these spectra.

By direct observation of the spectra in Figure 2, it is clear that the ν_s-CH_2 peak is barely noticeable in the spectra collected from water, the Na^+(aq), and the K^+(aq) solutions at ESP. To explain this finding, the VSFG selection rules are used. As a reminder, SFG is not active in a centrosymmetric medium; therefore, the observation of low intensity in the ν_s-CH_2 mode could be explained by assuming formation of centrosymmetry between any adjacent pair of CH_2 groups when the chains are in an all-trans conformation. With an even number of CH_2 groups as in PA, the pairing is more complete than another fatty acid with an odd number of CH_2 groups. Hence, this explanation has been widely accepted in the VSFG community on the basis of similar findings reported in other studies.[34] Furthermore, to reconfirm formation of a highly compact structure of the PA

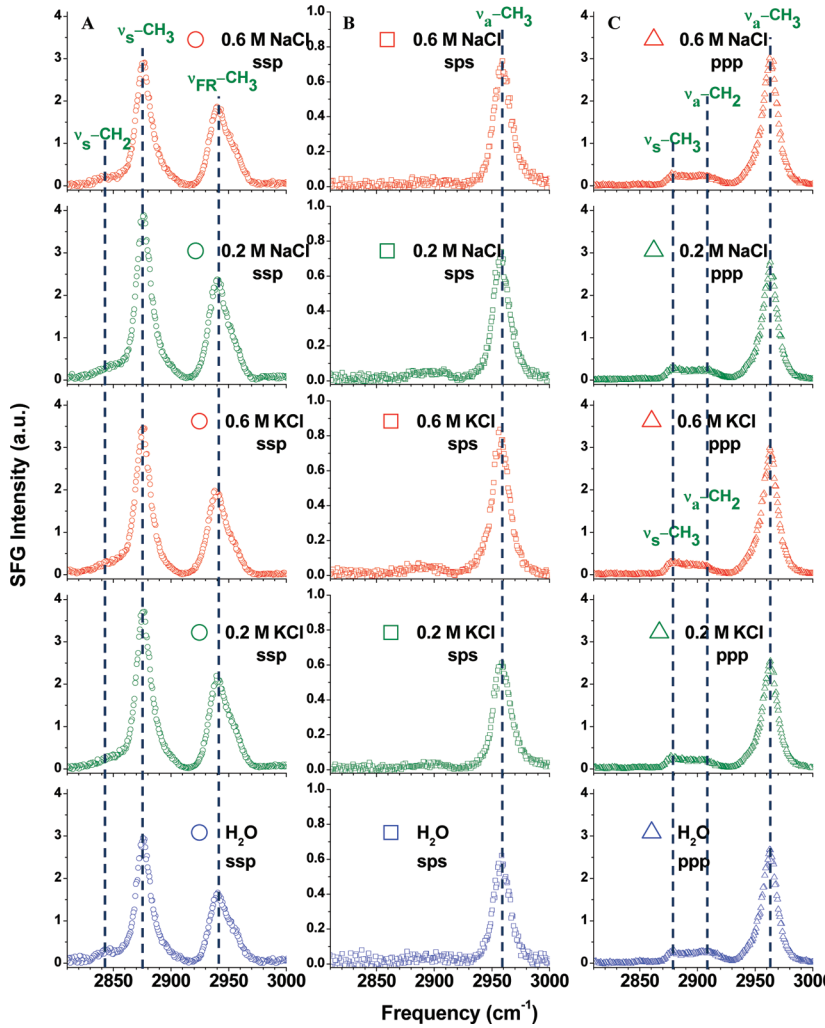

Figure 2. VSFG spectra of the PA monolayers on aqueous NaCl and KCl (0.2 and 0.6 M) solutions and neat water at ESP under three polarization combinations: (A) ssp, (B) sps, and (C) ppp; blue, green, and red colors denote the subphase of neat water and aqueous 0.2 and 0.6 M salt solutions, respectively. Vibrational modes of ν_s-CH_2, ν_s-CH_3, and ν_{FR}-CH_3 in (A), ν_a-CH_3 in (B), and ν_s-CH_3, ν_a-CH_2, and ν_a-CH_3 in (C) are shown in the spectra. Dashed lines are provided as a guide for the eye.

TABLE 1: Peak Assignments of VSFG Spectra of the PA Monolayers on Neat Water, NaCl, and KCl Solutions (0.2 and 0.6 M) at ESP for the Polarization Combinations ssp, sps, and ppp[a]

	CH_2-ss (cm^{-1})	CH_3-ss (cm^{-1})	CH_2-as (cm^{-1})	CH_3-FR (cm^{-1})	CH_3-as (cm^{-1})
ssp	2842	2872		2940	
sps			2910		2960
ppp		2872	2910		2960

[a] ss, symmetric stretch; as, asymmetric stretch; FR, Fermi resonance.

monolayer at ESP with close to surface normal orientation of the tails, the peak intensity ratio of $I_{\nu s\text{-}CH3}/I_{\nu s\text{-}CH2}$ in the ssp polarization combination is frequently used as a qualitative indicator to determine the orientation order of the PA tails with respect to the surface normal.[35,36] On the basis of our real-time in situ compression study coupled with VSFG, the acquired spectra of the PA monolayers on water, the Na^+(aq), and the K^+(aq) solutions reveal almost identical spectral features while obtained separately in the UC and collapse phase (spectra not shown). This confirms that monolayers at ESP are representative of the UC phase.

4.2.2. Carboxylate Symmetric Stretching (ν_s-COO^-) Region (1400−1500 cm^{-1}). Spectral investigations in the carboxylate stretching region have long been a hallmark in studies related to the ionic binding of metal ions with fatty acid headgroups, as often demonstrated by the IRRAS technique.[10,12,14] For the same purpose, special attention is paid to the PA monolayers on the Na^+(aq) and K^+(aq) solutions in this spectral region. First, to eliminate spectral contributions from the C—H bending modes, perdeuterated chains of PA (D_{31}-PA) were employed. In addition, a direct investigation of the deprotonated form of the carboxylate headgroups (—COO^-) was also implemented; namely, a pH study of the D_{31}-PA monolayers on a water surface was undertaken with pH values of 1.0, 6.0, and 13.3.

Initially ssp VSFG spectra of the D_{31}-PA monolayers on the water surface with different pH values were obtained separately, as illustrated in Figure 3. In looking at the spectrum at pH 13.3, an intense and symmetric peak centered at 1410 cm^{-1} is clearly observed. This is a direct indication of —COO^- groups within the interface. Under this highly basic condition, the carboxylate headgroups of D_{31}-PA should all be in the deprotonated form since the pK_a values of fatty acid homologues are generally reported in the range of 5−8.[14,22,37] In theory, to observe an SFG intensity, the molecules in the interface must show some degree of structural order and lack of inversion symmetry.

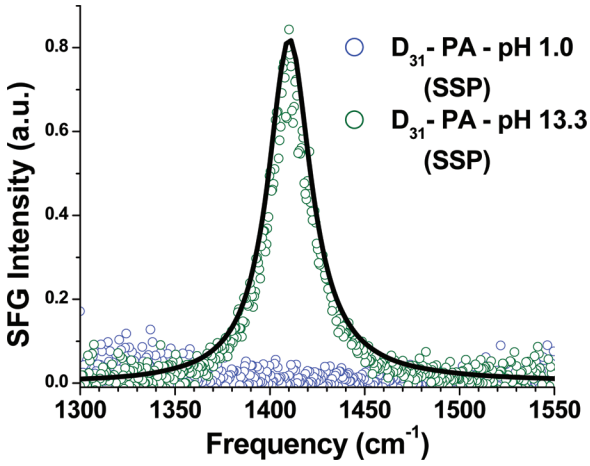

Figure 3. ssp VSFG spectra of the D_{31}-PA monolayers on water with pH values at 1.0 and 13.3. The fitted curve for the pH 13.3 spectrum is shown as a solid line.

Therefore, on the basis of the observed peak intensity, even at pH 13.3, the deprotonated form of the D_{31}-PA monolayer at ESP maintains its ordered structure with respect to the carboxylate headgroups. The hydrophobic tails are highly likely to impede any formation of cyclic dimers within the monolayer as is observed in acetic acid−water mixtures within the interface.[38] According to both bulk transmission and surface reflection IR studies reported in literature, the ν_s-COO^- peak is usually reported in the spectral range of 1400−1500 cm^{-1} for long-chain fatty acid monolayers in the deprotonated form on aqueous salt solutions that contain metal cations. However, in this spectral range, the reported IRRAS spectra are usually congested with multiple peaks originating from both the C−H bending modes and the ν_s-COO^- modes in different metal-specific coordination environments.[10,12] Here, taking advantage of VSFG and the isotopic substitution of PA, the 1410 cm^{-1} peak is solely visible. It is, therefore, reasonable to attribute this peak to the hydrated species of the $-COO^-$ groups that is prevalent in this environment. The aqueous solution is highly basic, as is the aqueous interface. (Note that the high pH studies utilize NaOH to control pH, but these concentrations are orders of magnitude smaller than those used in the salt studies.) The assignment to the hydrated species of the $-COO^-$ groups is in good agreement with the work done by Miranda et al. on hexacosanoic acid (C_{26} saturated fatty acid) under similar conditions.[15] At pH 1.0, there is no obvious spectral intensity from the D_{31}-PA monolayer in Figure 3. This can be easily explained by the fact that the majority of D_{31}-PA molecules exist in the protonated form at this pH and therefore have no contribution in this spectral range. In addition, the D_{31}-PA spectral response at pH 6.0 (data not shown) is similar to the one shown in pH 1.0, which may imply that the majority of monolayer constituents are still in the protonated form at this pH.

In Figure 4A,B, ssp VSFG spectra of the D_{31}-PA monolayers obtained from the Na^+(aq) and K^+(aq) solutions reveal considerable intensities in this spectral region. Two peaks with respective center-wavelength positions at 1414 and 1475 cm^{-1} are shown. In the absence of contributions from the C−H bending modes, the source of contributions to these two peaks is most likely from the $-COO^-$ groups that manifest into two distinct species. Upon considering the close proximity of the 1414 cm^{-1} peak to the one at 1410 cm^{-1} as identified previously, it is reasonable to assume that the former is also derived from the same molecular species that are characterized by the hydrated form of the $-COO^-$ groups. Even though the 1414 cm^{-1} peak appears to be broader than that observed at pH 13.3 in Figure 3, this could be accounted for by postulating that there exists a relatively fewer number of the $-COO^-$ groups that somehow are interdispersed among these protonated species to cause a population dispersion.[14] Furthermore, the presence of cations could also affect the hydration shells around the $-COO^-$ groups to induce a similar spectral broadening.

The higher frequency peak at ~1475 cm^{-1} shown in Figure 4A,B has also been found in similar studies by IRRAS, as demonstrated by Gericke et al.[10] This peak is mainly dominant with the K^+(aq) solutions (Figure 4B). Since complete isotopic substitution has been emphasized in our study, it is sensible to rule out the δ-CH_2 contribution, which leaves the only choice to the ionic complex form of the $-COO^-$ groups having interactions with Na^+ or K^+. Previously, ionic complexes and coordinated species have been identified in studies of metal ions binding to fatty acid monolayers using IRRAS.[10,14,39] In our work, complex formation of divalent cations with D_{31}-PA has also been recently observed evidenced by a peak that also appears at 1475 cm^{-1} (unpublished data). This recent observation suggests that this peak originates from the pure ionic complexes and bears no relation with the valency of the binding cations. On the contrary, the 1414 cm^{-1} peak associated with the hydrated species of the $-COO^-$ groups is much more dynamic in relation to the cation valency. We will report the divalent cation findings in an upcoming paper.

Most importantly, in looking at Figure 4A,B, it is apparent that the 1414 cm^{-1} peak only increases in the Na^+(aq) solutions when the concentration is increased from 0.2 to 0.6 M, while the 1475 cm^{-1} peak solely increases in the K^+(aq) solutions after following the same increase in concentration. According to our postulates, each peak is assigned to a different $-COO^-$ species, the 1414 cm^{-1} peak for the hydrated $-COO^-$ species and the 1475 cm^{-1} peak for the complexed $-COO^-$ species. To clarify these two assignments, some classical theories seem to work well. It is obvious that both Na and K belong to the alkali metals. In their common state of ionization they share closed shell electronic structures that show noble-gas-like chemistry. Therefore, it is important to note that, when they interact with the headgroup, they act like point charges with no distinguishable chemistry, which further dictates the interaction to be purely electrostatic. Because the charge density on K^+ is about half the value on Na^+, 0.045 versus 0.088 C/Å^3,[40] respectively, it is natural to imply that K^+ binds less tightly with surrounding water molecules than Na^+, which can be further supported by the difference in Stokes hydration radii of these two cations, 3.3 and 2.4 Å with respect to Na^+ and K^+.[40] Given this unique physical property, K^+ is more likely to interact with the headgroup than Na^+ during the diffusion-controlled process. Once a charge−dipole interaction is experienced both by a K^+ and by a headgroup, they are likely to bind strongly to allow the inner sphere substitution of water molecules to proceed. Ultimately, the headgroup is able to replace most of the water molecules in the first hydration shell of K^+. Then, deprotonation occurs, and a 1:1 ionic complex forms, $-COO^-/K^+$. This favors surface neutrality. In addition, the inner sphere substitution rate of the first hydration shell around K^+ is slightly faster than Na^+.[40] Therefore, the selective intensity trends depicted in Figure 4A,B seem reasonable in the systems that are investigated here.

Two points can be used to summarize the interesting observations discussed above. First, deprotonation of the headgroup can be initiated by the presence of metal cations in the

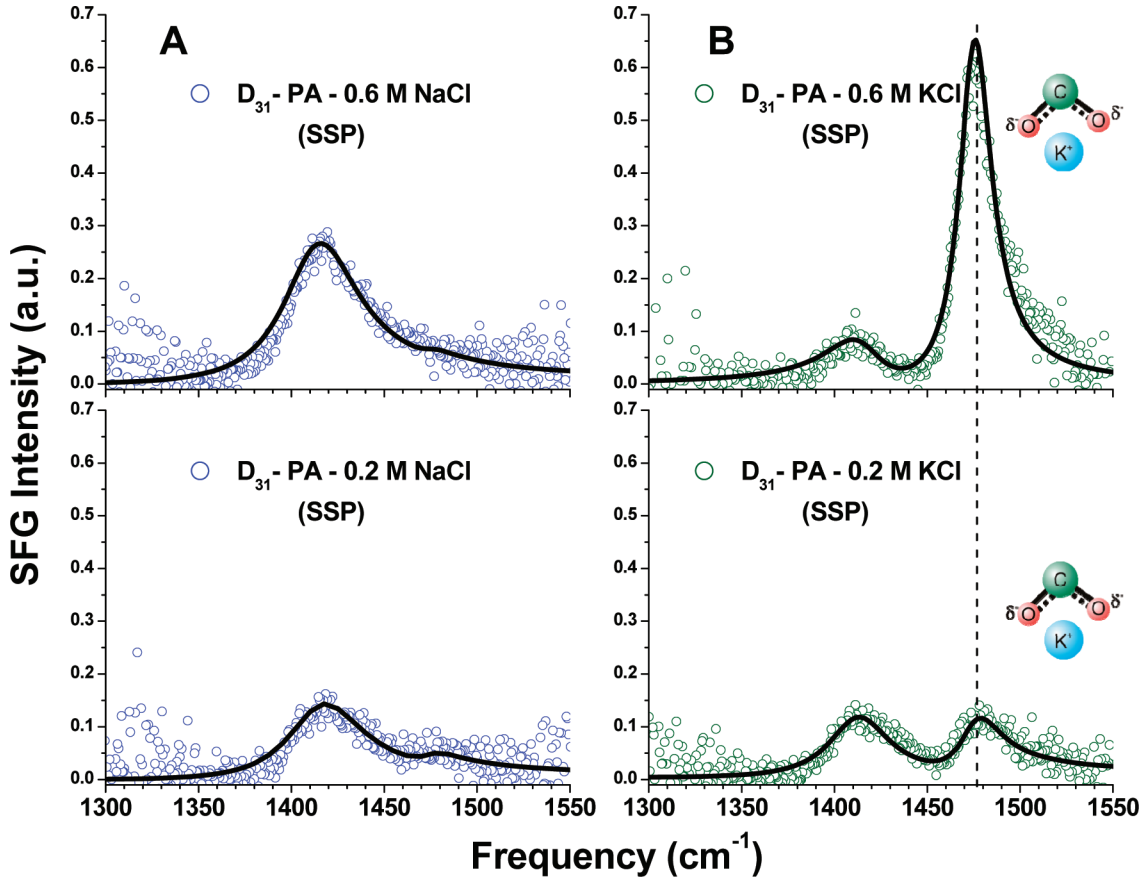

Figure 4. ssp VSFG spectra of the D_{31}-PA monolayers on salt solutions: (A) 0.2 and 0.6 M NaCl solutions and (B) 0.2 and 0.6 M KCl solutions. The individual fitted curves are shown as solid lines.

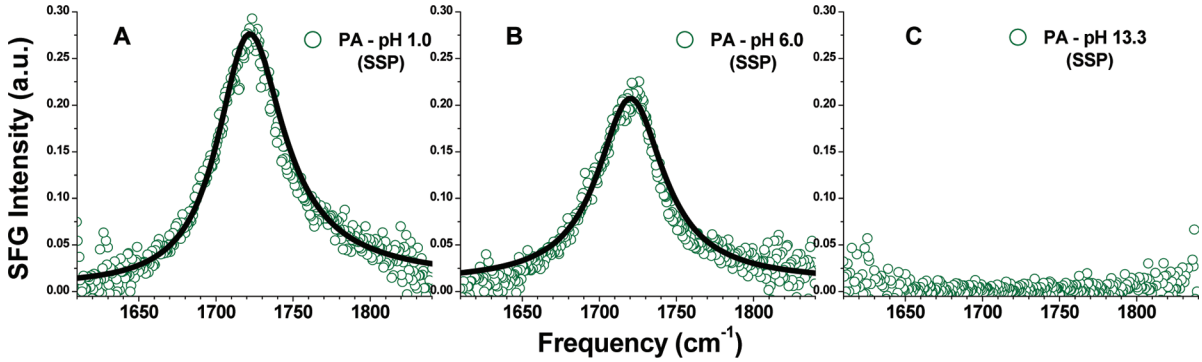

Figure 5. ssp VSFG spectra of the PA monolayers on water at pH values (A) 1.0, (B) 6.0, and (C) 13.3. The individual fitted curves are shown as solid lines.

aqueous solution. Second, the extent of ion complex formation is cation specific and also follows a nearly linear relationship with the cation concentration in the bulk with respect to K^+. This linearity indicates a 1:1 complex formation between K^+ and a $-COO^-$ group. In later sections of this paper, spectral evidence from other spectral regions also confirm these findings.

4.2.3. Carbonyl Stretching (ν-C═O) Region (1600−1800 cm^{-1}). To further support the spectral findings in the ν_s-COO^- stretching region presented in the previous section, VSFG spectra of the PA monolayers were acquired from the water surface under the same set of pH conditions (1.0, 6.0, and 13.3) in the C═O stretching region. Then, the same spectral investigations were conducted on the Na^+(aq) and K^+(aq) solutions, respectively.

One strong symmetric peak with its center-wavelength position at 1720 cm^{-1} is shown in Figure 5A,B, while there is no spectral intensity in Figure 5C. This is opposite to the observation shown in the ν_s-COO^- stretching region with respect to pH. First, it is important to point out that the only difference among these spectra is the pH value where (A) is the most acidic at pH 1.0, (C) is the most basic at pH 13.3, and (B) is close to neutral at pH 6.0. According to spectral assignments based on IR and Raman studies,[41] this peak is attributed to the C═O stretching mode in the protonated form of carboxylate headgroups (COOH). The presented spectra are consistent with the molecular constituents in the headgroups as expected at these pH conditions. As mentioned previously, the PA headgroup at pH values of 1.0 and 6.0 should be mostly protonated, and the degree of dissociation should be correlated with pH. Therefore, the population of the protonated headgroups at pH 1.0 should be higher than that at pH 6.0 even though at the near neutral pH most of headgroups are still protonated. Indeed, this trend

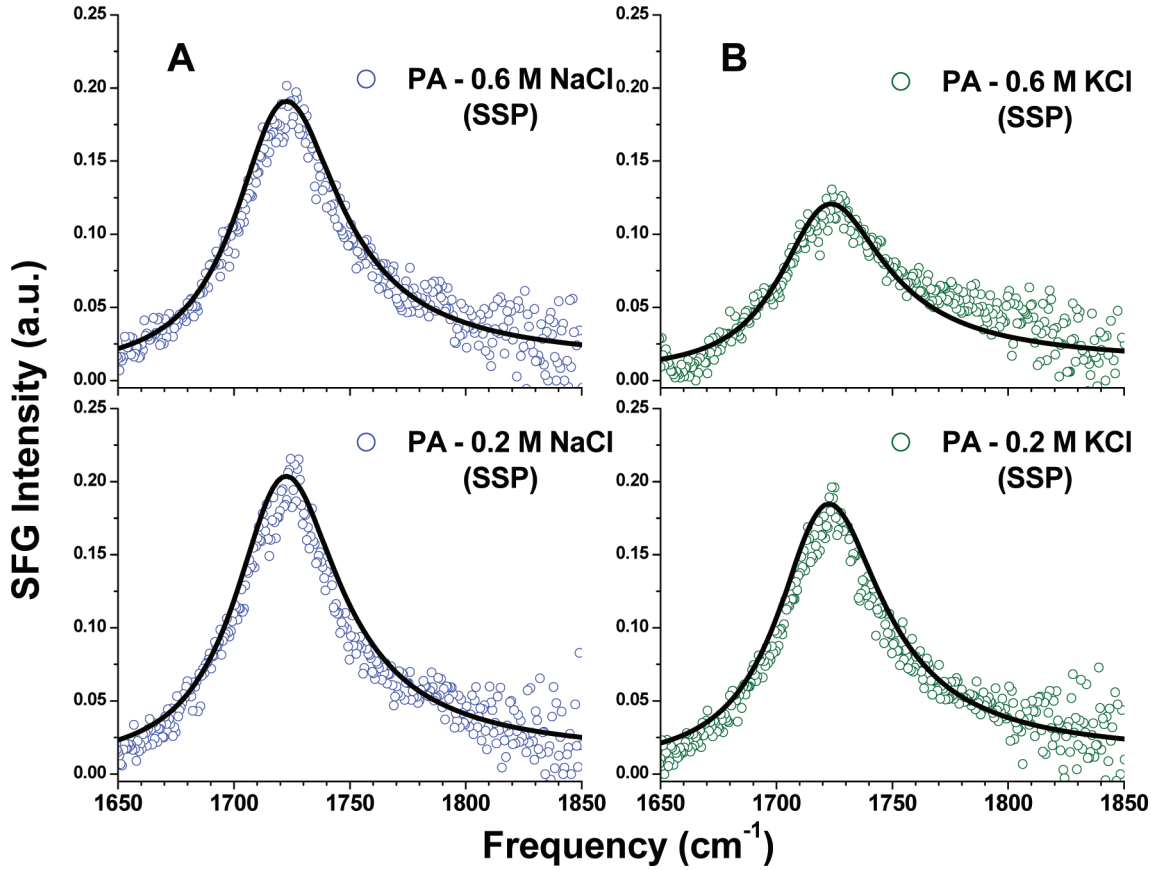

Figure 6. ssp VSFG spectra of the PA monolayers on salt solutions: (A) 0.2 and 0.6 M NaCl solutions and (B) 0.2 and 0.6 M KCl solutions. The individual fitted curves are shown as solid lines.

is strongly confirmed by observing a higher peak intensity in Figure 5A than that in Figure 5B. At pH 13.3, because of near complete deprotonation, PA headgroups are mostly transformed to the $-COO^-$ groups. Therefore, there should be no intensity in the C=O spectral region as shown in Figure 5C.

ssp VSFG C=O spectra of the PA monolayers acquired from the Na^+(aq) and K^+(aq) solutions are presented in Figure 6A,B. Clearly the single C=O peak appears in the Na^+(aq) and K^+(aq) solutions at 0.2 and 0.6 M, respectively. The respective spectral features of the observed peaks are identical in terms of the peak position and hwhm as denoted in the fitting parameters shown in eq 2. The peak intensity of the C=O peak in both Na^+(aq) solutions are almost identical, irrespective of the concentration difference. This indicates that the degree of deprotonation of the PA monolayers on the Na^+(aq) solutions may have an upper limit because having a strong hydration shell around each Na^+ is a roadblock for forming an ionic complex with the headgroup. On the other hand, the peak intensity variations observed in the K^+(aq) solutions show concentration dependence. For instance, by varying the concentration from 0.2 to 0.6 M in the K^+(aq) solutions, a significant peak intensity decrease takes place. It is reasonable to assume that this is mainly caused by deprotonation of the headgroup due to complex formation. To calculate the percent loss of the C=O groups when the concentration of K^+(aq) solution is increased from 0.2 to 0.6 M, we can normalize the overall peak intensity difference existing in the respective spectra over the one in the reference spectrum (here, the ν-C=O spectrum at 0.2 M). Because SFG intensity is proportional to N^2 (number density squared), the square root ratio of this normalized intensity is needed to quantify the corresponding percent loss in the number density. The calculated percent loss is 50%. On the other hand, this percent loss in theory should be consistent with the value that corresponds to the percent increase of the $-COO^-$ groups in the same solutions. To confirm this point, the same logic is applied to the spectra collected in the 1400−1500 cm^{-1} region, but it is necessary to bundle the two identified $-COO^-$ groups into one to account for the overall effect. The estimated value of the percent increase of the $-COO^-$ groups due to K^+ binding is 60%, which is slightly higher than the fitting value of 50% from the C=O stretching region.

4.2.4. O−H Stretching Region (3500−3800 cm^{-1}). As a complementary probe, the O−H stretch at the higher frequency side of the hydrogen bonding stretch region was also investigated. There is some consensus that a continuum of hydrogen bonding strengths exists from about 3000 to 3600 cm^{-1} as described in VSFG studies. In addition, the dangling O−H oscillators exist at ~3700 cm^{-1}.[28,42,43] In this part of investigation, first, the dangling O−H peak is used as a common reference in evaluating if there exists a different response of this mode to the separate presence of Na^+ and K^+ in the bulk aqueous solutions; second, special emphasis is placed on the broad 3590 cm^{-1} O−H stretching peak that is uniquely demonstrated in the aqueous interface with fatty acid coverage.

In Figure 7, ssp VSFG spectra of the neat water and the pure 0.6 M Na^+(aq) and K^+(aq) solutions in the dangling O−H stretching region of water are presented. A sharp peak with ~20 cm^{-1} (hwhm) at 3702 cm^{-1} is observed in all three spectra. These observed peaks are attributed to the dangling O−H oscillators of water molecules that reside at the very top layer of the hydrogen-bonded water network. These three spectra are almost identical, showing similar intensities. With this finding in mind, there is negligible surface perturbation from Na^+ and K^+ to the dangling O−H oscillators of water molecules, which

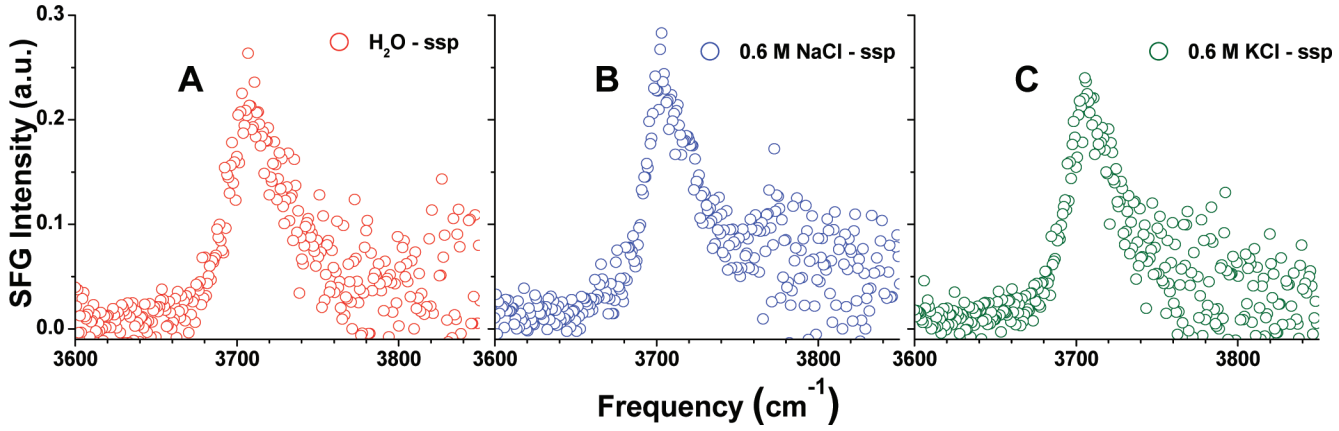

Figure 7. ssp VSFG spectra of neat water and pure salt solutions (without monolayer) showing the dangling OH of surface water molecules: (A) neat water, (B) 0.6 M NaCl solution, and (C) 0.6 M KCl solution.

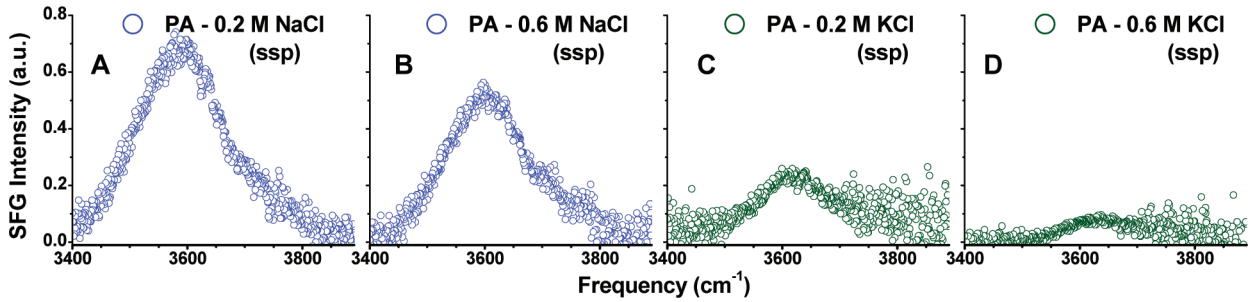

Figure 8. ssp VSFG spectra of the PA monolayers on salt solutions showing the OH of the PA carboxylic acid. PA spread on (A) 0.2 M NaCl solution, (B) 0.6 M NaCl solution, (C) 0.2 M KCl solution, and (D) 0.6 M KCl solution.

is consistent with the long-standing perception in classical theories that the alkali cations favor strong hydration shells and are inclined to be buried in the bulk. Therefore, no distinction exists in the pure Na^+(aq) and K^+(aq) solutions. However, by simply introducing a monolayer coverage of PA on these two solutions, interestingly, K^+ demonstrates a stronger complexion ability by causing more deprotonation in the headgroup as shown in the spectra presented in the previous sections. Additional spectral evidence is provided below confirming deprotonation induced by the ionic binding.

ssp VSFG spectra of the PA monolayers on the pure Na^+(aq) and K^+(aq) solutions (at 0.2 and 0.6 M) in the dangling O—H stretching region are shown in Figure 8. The common feature shared in these spectra is the manifestation of one broad peak which decreases in intensity, and its center-wavelength becomes blue-shifted (from 3590 to 3620 cm^{-1}) as shown in Figure 8. In previous SFG studies, the assignment of this peak has been unclear. For instance, this peak was first assigned to the OH stretch of weakly interacting OH groups between fatty acid (C_{26}) and water molecules by Miranda et al.[15] and recently was modified as the OH stretch of weakly or non-hydrogen-bonded water molecules by Johnson et al. in studies of acetic acid molecules.[38] Here, supported by more concrete spectral evidence acquired in this study, the former assignment is more reasonable. We assign this peak to the OH stretch of an isolated hydrogen-bonded OH of the COOH group and the hydrogen-bonded water OH. This mode arises only between the carboxylic acid headgroup and the water molecules. An absence of either of these deems the disappearance of this unique spectral signature. It is more important to address the aspect of deprotonation first before discussing this peak assignment.

Because this specific peak has OH stretch contributions from the PA headgroups (—COOH), this broad peak can also be used as a probe for monitoring the deprotonation event. In looking at the PA spectra acquired from the Na^+(aq) solutions at 0.2 and 0.6 M, it is evident that the peak intensity of the OH stretch is slightly stronger in the 0.2 M solution than that in the 0.6 M solution. The peak position at 3590 cm^{-1} does not shift. The loss of signal is attributed to the loss of OH oscillators, which is a direct result of deprotonation of the headgroup. In the Na^+(aq) solutions, deprotonation is infrequent. However, the headgroups that are deprotonated exist predominantly in their hydrated form. These headgroups should continue to contribute to the SFG signal in this region. This observation is consistent with the spectral data that we have observed in other spectral regions presented above.

The spectra of the PA monolayers collected from the K^+(aq) solutions (Figure 8C,D) show a more abrupt intensity decrease and a significant blue-shift of the peak position as the concentration is increased from 0.2 to 0.6 M. The significant intensity decrease has two related causes: first, the loss of the OH oscillators in the headgroup due to deprotonation and, second, complex formation. K^+ favors forming a 1:1 complex with the $—COO^-$ group as proposed previously. This is unlike Na^+. Once the complex is formed, it would act like a single entity that further prevents hydrogen-bonding with the surrounding water molecules.

In further evaluation of Figure 8, a 30 cm^{-1} blue-shift of the OH stretching peak in the K^+(aq) spectra relative to the Na^+(aq) spectra is observed. This is an indication of increasingly weaker hydrogen bonds between PA headgroups and water molecules. This observed shift could be caused by perturbations from the complexed $K^+/—COO^-$ species on nearby protonated PA molecules hydrogen-bonded with water molecules.

The VSFG spectrum of the PA monolayer on the water surface at pH 13.7, as shown in Figure 9, is critical for the assignment of the 3590 cm^{-1} peak and confirmation of the ionic complex formation. A peak at 3590 cm^{-1} is evident with

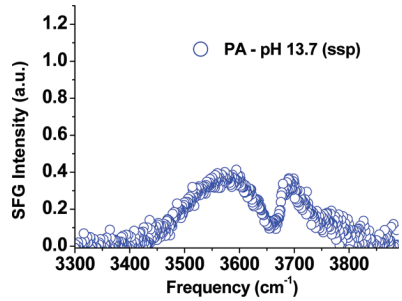

Figure 9. ssp VSFG spectra of the PA monolayers on neat water at pH 13.7 showing the hydrogen-bonded OH to PA and the dangling OH of surface water.

intensity similar to that of the near neutral pH (0.2 M K^+(aq) spectrum in Figure 8). A peak at ~3700 cm^{-1} is also observed (the dangling surface OH). The 3590 cm^{-1} peak is clearly not from the headgroup alone, because in this highly basic solution the majority of headgroups are in the deprotonated form. There is no —COOH. However, because of hydration, the 3590 cm^{-1} peak is observed, which indicates a direct and strong interaction between the deprotonated headgroups and the surrounding water molecules. On the other hand, as explained previously, a weaker peak or even the disappearance of this peak in the case of an ionic complex could be well reasoned by assuming that, once an ionic complex is formed, the interaction between the headgroup and the water molecules is greatly suppressed. The bound water molecules have been replaced by the cation in these cases. Given this reasoning, we come to the conclusion that the 3590 cm^{-1} peak is the unique product arising from water molecules directly interacting with the PA headgroups.

5. Conclusions

Ionic binding between the simple alkali metal cations and the fatty acid headgroups of PA can take place at the air—aqueous interface. Our findings indicate that alkali metal cations, in the case of Na^+ and K^+, have various degrees of binding affinities with the carboxylic acid headgroups of PA. On the neat water surface at a neutral pH, the majority of PA molecules are present in their protonated form, and deprotonation only occurs at relatively high basic conditions; however, this trend no longer holds when the aqueous phase contains simple alkali metal cations such as Na^+ and K^+, albeit at neutral conditions. The presence of these cations initiates deprotonation of the carboxylic acid headgroups via two unique mechanisms. First, the deprotonation of PA headgroups could be caused by the long-range electrostatic interaction between the hydrated cations and the headgroup; second, a similar interaction could as well directly result from ionic complex formation between the nonhydrated cations and the headgroup. To confirm these two unique mechanisms, our data imply that Na^+ favors the first mechanism, while K^+ tends to favor the second mechanism. This is consistent with the slight differences in their hydration parameters: surface charge and hydration radii. Moreover, the degree of overall acid deprotonation is significantly greater with K^+ than Na^+ because K^+ is more likely to form a 1:1 ionic complex with the $—COO^-$ groups.

On the basis of the significant findings presented in this study, it is important to note that K^+ binds more strongly to the headgroup of PA relative to Na^+ at the air—aqueous interface. Rather than direct charge interactions found in real biological systems controlled by physiological pH conditions, alkali metal cations such as K^+ can initiate deprotonation. This can occur at neutral pH. The K^+ ion then undergoes ionic complexation with biologically relevant chelating ligands, such as carboxylate groups.

It is clear that the results presented in this study are contrary to the findings obtained by other groups as previously mentioned. Saykally et al. studied individual ionic binding characteristics of Li^+, Na^+, and K^+ to formate and acetate counterions in bulk aqueous solution by identifying the corresponding spectral shifts of carbon K-edge spectra of C═O. Later, Winter et al. furthered the research to include NH_4^+ in the cation list and replaced the formate ion with glycine. Instead of probing the carbon K-edge spectral shift, the magnitudes of the peak intensity of the oxygen in the carboxylate group ($—COO^-$) were used to determine the relative ionic binding affinity of cations to the carboxylate anion. However, no direct comparisons can be established here because the chemical system used in our study and others[26,27] is somehow different: fatty acid monolayer systems at the air—aqueous interface in our case versus simple organic acid salts in aqueous solutions used by others.[26,27] Furthermore, the probing technique employed in this study is also different from that used by others,[26,27] which inherently leads to different specificity. VSFG is a surface specific probe, whereas XAS is predominantly a bulk probe. In an attempt to elucidate these opposing findings, the most fundamental factor could well lie on the possible difference between how Na^+ and K^+ behave in bulk versus how they behave in interfacial environments. Monolayer coverage of a fatty acid could well induce the very opposite binding characteristics of K^+ and Na^+ at the interface as compared with the observed binding behaviors of these two ions to the short-chain carboxylate groups in the bulk. With this in mind, these opposite findings may suggest that the true nature of ionic binding in real biological systems is not as simple as ligand-specific ionic interactions.

Acknowledgment. We thank NSF (Chemistry Division, CHE-0749807) and a Camille Dreyfus Teacher-Scholar Award for financial support of this work.

Supporting Information Available: VSFG ppp polarized spectra in the COO^- and the OH stretching regions. This material is available free of charge via the Internet at http://pubs.acs.org.

References and Notes

(1) *Biological Membrane Ion Channnels Dynamics, Structure, and Applications*; Chung, S.-H., Andersen, O. S., Krishnamurthy, V., Eds.; Springer: New York, 2007.

(2) Lodish, H.; Berk, A.; Matsudaira, P.; Kaiser, C. A.; Krieger, M.; Scott, M. P.; Zipursky, L.; Darnell, J. *Molecular Cell Biology*, 5th ed.; W. H. Freeman: New York, 2003.

(3) Fendler, J. H. *Membrane Mimetic Chemistry: Characterizations and Applications of Micelles, Microemulsions, Monolayers, Bilayers, Vesicles, Host-guest Systems, and Polyions*; Wiley-Interscience: New York, 1982.

(4) Ma, G.; Allen, H. C. *Langmuir* **2007**, *23*, 589.

(5) Kaganer, V. M.; Peterson, I. R.; Kenn, R. M.; Shih, M. C.; Durbin, M.; Dutta, P. *J. Chem. Phys.* **1995**, *102*, 9412.

(6) Zhuang, X.; Miranda, P. B.; Kim, D.; Shen, Y. R. *Phys. Rev. B* **1999**, *59*, 12632.

(7) Henon, S.; Meunier, J. *Rev. Sci. Instrum.* **1991**, *62*, 936.

(8) Lipp, M. M.; Lee, K. Y. C.; Zasadzinski, J. A.; Waring, A. J. *Rev. Sci. Instrum.* **1997**, *68*, 2574.

(9) Lipp, M. M.; Lee, K. Y. C.; Waring, A.; Zasadzinski, J. A. *Biophys. J.* **1997**, *72*, 2783.

(10) Simon-Kutscher, J.; Gericke, A.; Huhnerfuss, H. *Langmuir* **1996**, *12*, 1027.

(11) Adamson, A. W.; Gast, A. P. *Physical Chemistry of Surfaces*, 6th ed.; Wiley-Interscience: New York, 1997.

(12) Wang, Y. C.; Du, X. Z.; Guo, L.; Liu, H. J. *J. Chem. Phys.* **2006**, *124*, 9.

(13) Dluhy, R. A.; Cornell, D. G. *J. Phys. Chem.* **1985**, *89*, 3195.
(14) Le Calvez, E.; Blaudez, D.; Buffeteau, T.; Desbat, B. *Langmuir* **2001**, *17*, 670.
(15) Miranda, P. B.; Du, Q.; Shen, Y. R. *Chem. Phys. Lett.* **1998**, *286*, 1.
(16) Chen, X.; Yang, T.; Kataoka, S.; Cremer, P. S. *J. Am. Chem. Soc.* **2007**, *129*, 12272.
(17) Zhang, Y. J.; Cremer, P. S. *Curr. Opin. Chem. Biol.* **2006**, *10*, 658.
(18) Schrodle, S.; Moore, F. G.; Richmond, G. L. *J. Phys. Chem. C* **2007**, *111*, 8050.
(19) Sovago, M.; Wurpel, G. W. H.; Smits, M.; Muller, M.; Bonn, M. *J. Am. Chem. Soc.* **2007**, *129*, 11079.
(20) Bian, H.-T.; Feng, R.-R.; Guo, Y.; Wang, H.-F. *J. Chem. Phys.* **2009**, *130*, 134709.
(21) Feng, R.-R.; Bian, H.-T.; Guo, Y.; Wang, H.-F. *J. Chem. Phys.* **2009**, *130*, 134710.
(22) Konek, C. T.; Musorrafiti, M. J.; Al-Abadleh, H. A.; Bertin, P. A.; Nguyen, S. T.; Geiger, F. M. *J. Am. Chem. Soc.* **2004**, *126*, 11754.
(23) Vrbka, L.; Vondrasek, J.; Jagoda-Cwiklik, B.; Vacha, R.; Jungwirth, P. *Proc. Natl. Acad. Sci. U.S.A.* **2006**, *103*, 15440.
(24) Vlachy, N.; Jagoda-Cwiklik, B.; Vacha, R.; Touraud, D.; Jungwirth, P.; Kunz, W. *Adv. Colloid Interface Sci.* **2009**, *146*, 42.
(25) Shen, Y. R. *The Principles of Nonlinear Optics*; Wiley-Interscience: New York, 1984.
(26) Uejio, J. S.; Schwartz, C. P.; Duffin, A. M.; Drisdell, W. S.; Cohen, R. C.; Saykally, R. J. *Proc. Natl. Acad. Sci. U.S.A.* **2008**, *105*, 6809.
(27) Aziz, E. F.; Ottosson, N.; Eisebitt, S.; Eberhardt, W.; Jagoda-Cwiklik, B.; Vacha, R.; Jungwirth, P.; Winter, B. *J. Phys. Chem. B* **2008**, *112*, 12567.
(28) Richmond, G. L. *Chem. Rev.* **2002**, *102*, 2693.
(29) Finlayson-Pitts, B. J. *J. Chem. Educ.* **1992**, *69*, 559.
(30) Hommel, E. L.; Ma, G.; Allen, H. C. *Anal. Sci.* **2001**, *17*, 1325.
(31) Kaganer, V. M.; Mohwald, H.; Dutta, P. *Rev. Mod. Phys.* **1999**, *71*, 779.
(32) Kajiyama, T.; Oishi, Y.; Uchida, M.; Tanimoto, Y.; Kozuru, H. *Langmuir* **1992**, *8*, 1563.
(33) Linden, M.; Rosenholm, J. B. *Langmuir* **1995**, *11*, 4499.
(34) Ma, G.; Allen, H. C. *Langmuir* **2006**, *22*, 5341.
(35) Conboy, J. C.; Messmer, M. C.; Richmond, G. L. *J. Phys. Chem.* **1996**, *100*, 7617.
(36) Walker, R. A.; Conboy, J. C.; Richmond, G. L. *Langmuir* **1997**, *13*, 3070.
(37) Betts, J. J.; Pethica, B. A. *Trans. Faraday Soc.* **1956**, *52*, 1581.
(38) Johnson, C. M.; Tyrode, E.; Baldelli, S.; Rutl, M. W.; Leygraf, C. *J. Phys. Chem. B* **2005**, *109*, 321.
(39) Gericke, A.; Huhnerfuss, H. *Thin Solid Films* **1994**, *245*, 74.
(40) *Inorganic Biochemistry II*; Kustin, K., McLeod, G. C., Renger, G., Burgermeister, W., Winkler-Oswatitsch, R., Eds.; Springer-Verlag: Berlin, 1977; Vol. 69.
(41) Genin, F.; Quiles, F.; Burneau, A. *Phys. Chem. Chem. Phys.* **2001**, *3*, 932.
(42) Gopalakrishnan, S.; Liu, D.; Allen, H. C.; Kuo, M.; Shultz, M. J. *Chem. Rev.* **2006**, *106*, 1155.
(43) Du, Q.; Superfine, R.; Freysz, E.; Shen, Y. R. *Phys. Rev. Lett.* **1993**, *70*, 2313.

JP9000434